This article has been accepted for publication in a future issue of this journal, but has not been fully edited. Content may change prior to final publication. Citation information: DOI 10.1109/TPEL.2018.2841206, IEEE Transactions on Power Electronics

Comments on "Digital Current Control in a Rotating Reference Frame-Part I: System Modeling and the Discrete Time-Domain Current Controller With Improved Decoupling Capabilities"

Claudio A. Busada, Sebastian Gomez Jorge† and Jorge A. Solsona, *Senior Member, IEEE*
All authors are with the the Instituto de Investigaciones en Ingeniería Eléctrica (IIIE), Universidad Nacional del Sur (UNS)-CONICET and Dpto. Ing. Eléctrica y de Computadoras, UNS, Av. Alem 1253, (8000) Bahía Blanca, Argentina.
(e-mail: cbusada@uns.edu.ar; sebastian.gomezjorge@uns.edu.ar; jsolsona@uns.edu.ar).
† Corresponding author: Dr. Sebastian Gomez Jorge

***Abstract*—A recent paper presents a discrete time model in a rotating dq reference frame of an R-L filter, and its current control. The purpose of this note is: 1) To show that the discrete model presented in the paper behaves differently to the sampled continuous time model of the plant, formulated in the stationary $\alpha\beta$ reference frame. 2) To find the proper discretization of the plant in dq coordinates. 3) To verify that there is cross coupling between axis d and q in the closed loop system if the original model is used, and that this coupling is not present when using the model found in this note. In the note it is verified that having a precise model of the plant allows to fulfill the control objective of obtaining the complete decoupling between axis.**

***Index Terms*—Current control, digital modulation, discrete-time systems**

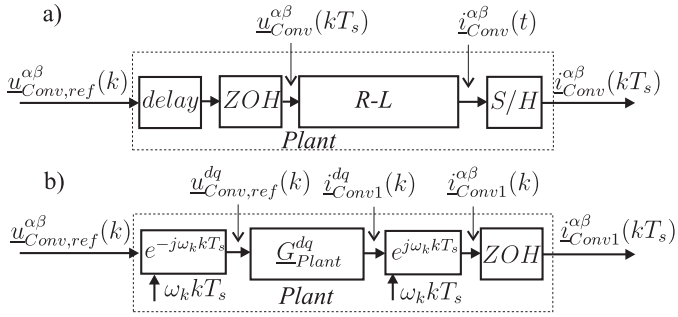

Fig. 1: System model. a) $\alpha\beta$ model. b) dq model.

I. Introduction

The authors of [1] propose a current controller with improved decoupling capabilities, formulated in a rotating dq reference frame. Unlike in [2], where the system is modeled in continuous time (a delay, for example, is modeled through a simple first order transfer function), in [1] great attention is given to the exact discrete time-domain modeling of the system. The exact system modeling gives rise to a new current controller structure that, ideally, allows the total decoupling between dq axis in the closed loop system. The system to be controlled is an R-L series circuit, described briefly in $\alpha\beta$ coordinates by:

$$\underline{u}^{\alpha\beta}_{Conv}(t) = R_1 \underline{i}^{\alpha\beta}_{Conv}(t) + L_1 \frac{d}{dt} \underline{i}^{\alpha\beta}_{Conv}(t), \tag{1}$$

where $\underline{i}^{\alpha\beta}_{Conv}(t)$ and $\underline{u}^{\alpha\beta}_{Conv}(t)$ represent the current and voltage in the circuit, respectively. This system is characterized by transfer function $\underline{G}^{\alpha\beta}_{LF}(s) = \underline{I}^{\alpha\beta}_{Conv}(s)/\underline{U}^{\alpha\beta}_{Conv}(s)$ (where the uppercase variable denotes Laplace transform of the lowercase variable). This R-L circuit is driven by a digitally controlled inverter, whose reference input is $\underline{u}^{\alpha\beta}_{Conv,ref}(k)$. Figure 1a shows a block diagram of the system, where discrete variables depend on k, while continuous variables depend on t or kT_s. In this figure, block $R-L$ represents system (1). Block ZOH represents the zero-order hold action produced by the PWM modulator, which is updated once per sampling cycle T_s. Block $delay$ represents the delay time T_d that occurs between the sampling time of signal $\underline{i}^{\alpha\beta}_{Conv}(t)$ at $t = kT_s$, and the time at which the control action $\underline{u}^{\alpha\beta}_{Conv,ref}(k)$ is effectively applied to the R-L filter. Block $Plant$ shown in Fig. 1a includes these three blocks.

In [1], a discrete time model of block $Plant$ of Fig. 1a is presented. This model is formulated in a dq reference frame rotating at angular frequency ω_k. Two delay cases are considered there: $T_d = T_s$ and $T_d = T_s/2$. The case where $T_d = T_s$ appears in symmetrical PWM with sampling at the start of each carrier period, and in asymmetrical PWM with sampling at the start and in the middle of each carrier period. The case where $T_d = T_s/2$ appears in symmetrical PWM with sampling in the middle of each carrier period (see [1] for more details). Figure 1b shows a schematic of the model presented in [1], represented by block $\underline{G}^{dq}_{\text{plant}}$. Block $e^{-j\omega_k kT_s}$ transforms the digital reference input $\underline{u}^{\alpha\beta}_{Conv,ref}(k)$ into $\underline{u}^{dq}_{Conv,ref}(k)$, while block $e^{j\omega_k kT_s}$ transforms $\underline{i}^{dq}_{Conv1}(k)$ into $\underline{i}^{\alpha\beta}_{Conv1}(k)$. Block $\underline{G}^{dq}_{\text{plant}}$ in Fig. 1b is characterized by transfer function $\underline{G}^{dq}_{\text{plant}}(z) = \underline{I}^{dq}_{Conv1}(z)/\underline{U}^{dq}_{Conv,ref}(z)$. In [1] [eqn. (25)], for $T_d = T_s$, the following transfer function is presented:

$$\underline{G}^{dq}_{\text{plant}}(z) = \frac{\overbrace{(1-\alpha_1)e^{-j\omega_k T_s}}^{K_s}}{R_1 + j\omega_k L_1} \frac{1}{z(z-\alpha_1)} = \frac{K_s}{z(z-\alpha_1)}, \tag{2}$$

This work was supported by Universidad Nacional del Sur, CONICET and ANPCyT, Argentina.

This article has been accepted for publication in a future issue of this journal, but has not been fully edited. Content may change prior to final publication. Citation information: DOI 10.1109/TPEL.2018.2841206, IEEE Transactions on Power Electronics

where $\alpha_1 = e^{-(\frac{1}{\tau_1}+j\omega_k)T_s} \in C$, and $\tau_1 = L_1/R_1$. Also in [1] [eqn. (26)], for $T_d = T_s/2$ the following transfer function is presented:

$$\underline{G}^{dq}_{\text{plant}}(z) = \frac{(1-\alpha_2)e^{-j\frac{1}{2}\omega_k T_s}}{R_1 + j\omega_k L_1}\frac{(z+\alpha_2)}{z(z-\alpha_1)}, \quad (3)$$

where $\alpha_2 = e^{-(\frac{1}{\tau_1}+j\omega_k)\frac{T_s}{2}} \in C$.

If block $\underline{G}^{dq}_{\text{plant}}$ in Fig. 1b is properly modeled, then $\underline{i}^{\alpha\beta}_{Conv1}(kT_s) = \underline{i}^{\alpha\beta}_{Conv}(kT_s)\ \forall k$ must be satisfied. In this letter it will be shown that (2) and (3) do not satisfy this condition, and the appropriate model, which does satisfy it, will be found. To further show the effect of each model in the closed loop behaviour, both models will be used in the design of the SRF-PI proposed in [1]. It will be shown that the closed loop system results decoupled in dq only when the model found in this note is used in the design of the controller. These results will be validated through simulation and experimental tests.

II. Testing the models

Figure 2a shows the simulation of the continuous time model of the plant of Fig. 1a, for $L_1 = 6mHy$, $R_1 = 0.36\Omega$, $T_d = T_s = 0.74ms$. These values of R_1 and L_1 are obtained from [1], and are used in all the simulations. The initial conditions are set to zero, and an input is set to $\underline{u}^{\alpha\beta}_{Conv,ref}(k) = 10V\cos(\omega_k kT_s) + j10V\sin(\omega_k kT_s)$, with $\omega_k = 2\pi 50$rad/s. With this choice it turns out that $\omega_s/\omega_k = 27$ (with $\omega_s = 2\pi/T_s$), the same situation considered in [1]. The thin lines in Fig. 2a show analog outputs $\underline{i}^{\alpha\beta}_{Conv}(t)$ of Fig. 1a, whereas the thick lines show outputs $\underline{i}^{\alpha\beta}_{Conv}(kT_s)$ after the sample and hold.

The system of Fig. 1b is simulated assuming $\underline{G}^{dq}_{\text{plant}}$ modeled by (2), with the same test input used to obtain Fig. 2a. Comparing the sampled outputs of both systems, it results that $\underline{i}^{\alpha\beta}_{Conv1}(k) \neq \underline{i}^{\alpha\beta}_{Conv}(k)$. Figure 2b shows the resulting error signal $\underline{e}^{\alpha\beta}(k) = \underline{i}^{\alpha\beta}_{Conv1}(k) - \underline{i}^{\alpha\beta}_{Conv}(k)$. This means that (2) does not properly model the plant in the rotating dq frame.

Figures 2d-e show the same results as Figs. 2a-b for the case where $T_d = T_s/2$ and $\underline{G}^{dq}_{\text{plant}}$ is modeled by (3). Figure 2e shows that (3) does not properly model the plant in dq coordinates either.

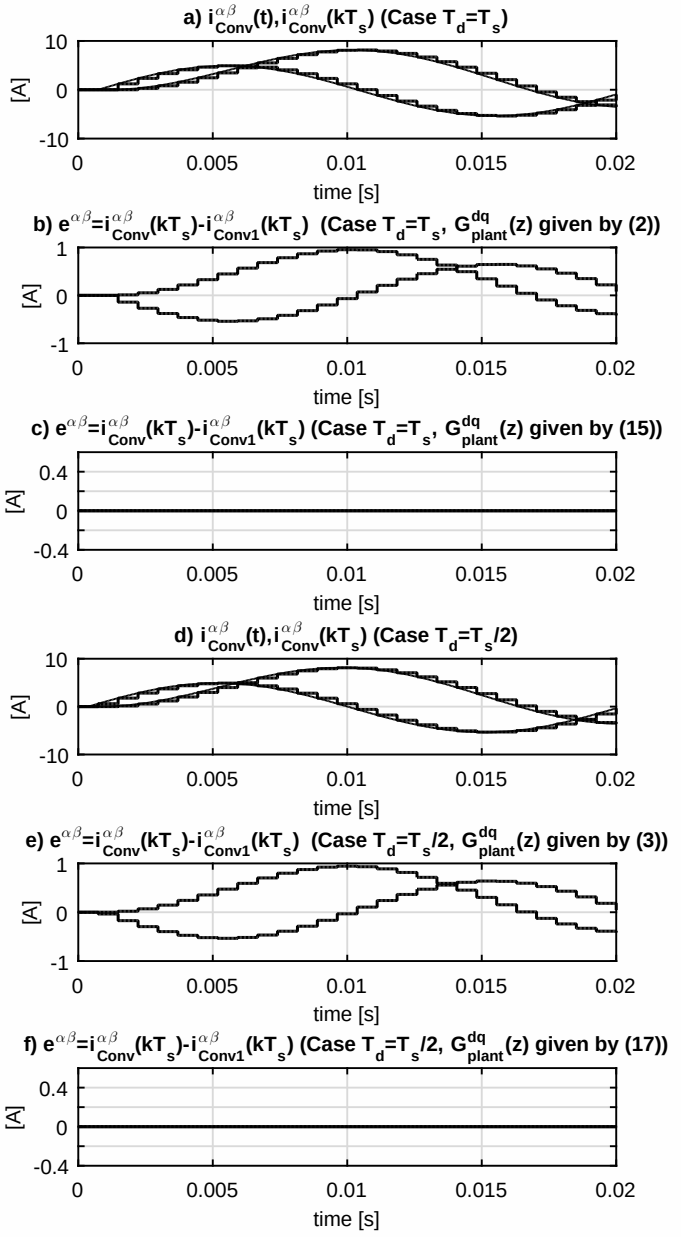

Fig. 2: Simulation results for the open loop plant of Fig. 1.

III. Model in dq coordinates

In this section, alternative dq models to those proposed in (2) and (3) are obtained. As will be shown, these models copy the behavior of block $Plant$ of Fig. 1a. Two methods will be used to obtain these models. The first one is the same method used in [1] for the case where $T_d = T_s$. The second method is used for the case where $T_d = T_s/2$, and is described below.

A. Case $T_d = T_s$

Let $T_d = T_s$, and follow the discretization method used in [1]. Block $delay$ of Fig. 1 has the following representation in the $\alpha\beta$ frame:

$$\underline{G}^{\alpha\beta}_{\text{sample}\to\text{update}}(s) = e^{-sT_d}. \quad (4)$$

The dq representation of this block, $\underline{G}^{dq}_{\text{sample}\to\text{update}}(s)$, is found in [1], [eqn. (18)]:

$$\underline{G}^{dq}_{\text{sample}\to\text{update}}(s) = e^{-sT_d}e^{-j\omega_k T_d}. \quad (5)$$

Therefore, the dq representation of block $delay$ is simply its $\alpha\beta$ representation multiplied by rotation $e^{-j\omega_k T_d}$.

Block ZOH of Fig. 1a is implemented in the stationary reference frame. This block models the fact that the PWM reference voltage is updated only once per sampling period T_s. Its transfer function in the $\alpha\beta$ reference frame is [3]:

$$\underline{G}^{\alpha\beta}_{\text{zoh}}(s) = \frac{1-e^{-sT_s}}{s}. \quad (6)$$

The ZOH consists of a delay and an integrator. Since it is a decoupled system in $\alpha\beta$, it must be coupled in dq. To obtain its model in dq coordinates, the dynamics of (6) must be trans-

This article has been accepted for publication in a future issue of this journal, but has not been fully edited. Content may change prior to final publication. Citation information: DOI 10.1109/TPEL.2018.2841206, IEEE Transactions on Power Electronics

formed to dq coordinates through the transformation defined in [1] [eqn. (5)]. Transfer function (6) in dq coordinates can be found simply by substituting the s operator in (6) by $s+j\omega_k$ [4]:

$$\underline{G}^{dq}_{\text{zoh}}(s)=\frac{1-e^{-sT_s}e^{-j\omega_k T_s}}{s+j\omega_k}. \tag{7}$$

This transfer function is different to the expression obtained in [1] [eqn. (19)]:

$$\underline{G}^{dq}_{\text{zoh}}(s)=\frac{1-e^{-sT_s}}{s}. \tag{8}$$

As can be seen, this equation is the same as (6), which is the $\alpha\beta$ description of block ZOH of Fig. 1a. Therefore, in [1] block ZOH is applied to a signal already in the dq frame, which is different to the reality shown in Fig. 1a. In the physical implementation of the system, block ZOH is applied to signal $\underline{u}^{\alpha\beta}_{Conv,ref}(k)$, which is in the $\alpha\beta$ frame. The difference between (7) and [eqn. (19)] of [1] is the reason why the signal $\underline{e}^{\alpha\beta}(k)\neq 0$, in Fig. 2b.

The model of block $Plant$ of Fig. 1a in dq coordinates, $\underline{G}^{dq}_{\text{plant}}(s)$, also contains the model of the R-L circuit in dq coordinates, $\underline{G}^{dq}_{L,F}(s)$, defined in [1] [eqn. (19)]:

$$\underline{G}^{dq}_{L,F}(s)=\frac{1}{R_1}\frac{1}{1+s\tau_1+j\omega_k\tau_1}, \tag{9}$$

Then, it results that:

$$\underline{G}^{dq}_{\text{plant}}(s)=\underline{G}^{dq}_{\text{zoh}}(s)\underline{G}^{dq}_{L,F}(s)\underline{G}^{dq}_{\text{sample}\rightarrow\text{update}}(s). \tag{10}$$

The $\mathcal{Z}$ transform of (10) is:

$$\underline{G}^{dq}_{\text{plant}}(z)=\mathcal{Z}\left\{\mathcal{L}^{-1}\left\{\underline{G}^{dq}_{\text{plant}}(s)\right\}\Big|_{t=kT_s}\right\}. \tag{11}$$

Replacing (5), (7) and (9) in (11), and assuming $T_d=T_s$ it results:

$$\underline{G}^{dq}_{\text{plant}}(z)=\frac{z-e^{-j\omega_k T_s}}{z^2}\mathcal{Z}\left\{\mathcal{L}^{-1}\left\{\underline{G}^{'dq}_{\text{plant}}(s)\right\}\Big|_{t=kT_s}\right\}, \tag{12}$$

where:

$$\underline{G}^{'dq}_{\text{plant}}(s)=\frac{e^{-j\omega_k T_s}}{R_1\tau_1}\frac{1}{(s+\frac{1}{\tau_1}+j\omega_k)(s+j\omega_k)}. \tag{13}$$

Using a $\mathcal{Z}$ transform table, the transformation of (13) results:

$$\underline{G}^{'dq}_{\text{plant}}(z)=\frac{e^{-2j\omega_k T_s}}{R_1}\frac{z(1-e^{-\frac{T_s}{\tau_1}})}{[z-e^{-(\frac{1}{\tau_1}+j\omega_k)T_s}](z-e^{-j\omega_k T_s})}. \tag{14}$$

Replacing this result in (12) the following equation is obtained:

$$\underline{G}^{dq}_{\text{plant}}(z)=\frac{\overbrace{(1-e^{-\frac{T_s}{\tau_1}})e^{-2j\omega_k T_s}}^{K_{s1}}}{R_1}\frac{1}{z(z-\alpha_1)}=\frac{K_{s1}}{z(z-\alpha_1)}, \tag{15}$$

where $\alpha_1=e^{-(\frac{1}{\tau_1}+j\omega_k)T_s}$. This is the required transfer function. The resulting model (15) matches the model found in [5], and also the more general model used in [6] (for $T_d=0$). These models were found through a different analytical method.

Comparing (15) with (2), it is noted that both have the same poles, but the complex constant of their numerator is different, $K_{s1}\neq K_s$. To verify the validity of (15), the simulation performed to obtain Fig. 2b was repeated using (15). The results are shown in Fig. 2c. Here, it can be seen that $\underline{e}^{\alpha\beta}(k)=0\ \ \forall k$, verifying the validity of (15).

B. Case $T_d=T_s/2$

In [1] the continuous time plant is transformed from the stationary $\alpha\beta$ frame to the rotating dq frame, then it is discretized. For the case where $T_d=T_s/2$ a different method is proposed here. The plant is discretized in the stationary $\alpha\beta$ frame, and then the resulting discrete model is transformed to the dq frame.

It is easy to verify, through integration of its differential equation, that the discretization of first order system (1) with $T_d=T_s/2$ results:

$$\underline{i}^{\alpha\beta}_{Conv}(k+1)=e^{-\frac{T_s}{\tau_1}}\underline{i}^{\alpha\beta}_{Conv}(k)+\frac{(1-e^{-\frac{T_s}{2\tau_1}})}{R_1}[\\ e^{-\frac{T_s}{2\tau_1}}\underline{u}^{\alpha\beta}_{Conv,ref}(k-1)+\underline{u}^{\alpha\beta}_{Conv,ref}(k)]. \tag{16}$$

It is known that if $\underline{x}$ is a generic complex magnitude, the dq and $\alpha\beta$ representations of $\underline{x}$ are related through: $\underline{x}^{dq}(k)=\underline{x}^{\alpha\beta}(k)e^{-j\theta(k)}$, $\underline{x}^{dq}(k+1)=\underline{x}^{\alpha\beta}(k+1)e^{-j[\theta(k)+\omega_k T_s]}$, where $\theta(k)$ is the angle between d and α axis, at time $t=kT_s$, and ω_k is the mean rotation angular frequency of the dq frame during the interval k to $k+1$. Transforming (16) to the dq frame, using this transformation, it results:

$$\underline{i}^{dq}_{Conv}(k+1)=\alpha_1\underline{i}^{dq}_{Conv}(k)+\frac{(1-e^{-\frac{T_s}{2\tau_1}})e^{-j\omega_k T_s}}{R_1}[\\ e^{-(\frac{T_s}{2\tau_1}+j\omega_k T_s)}\underline{u}^{dq}_{Conv,ref}(k-1)+\underline{u}^{dq}_{Conv,ref}(k)],$$

where $\alpha_1=e^{-(\frac{1}{\tau_1}+j\omega_k)T_s}$. Performing the $\mathcal{Z}$ transform of this last equation, the desired model is obtained:

$$\underline{G}^{dq}_{\text{plant}}(z)=\frac{(1-e^{-\frac{T_s}{2\tau_1}})e^{-j\omega_k T_s}}{R_1}\frac{(z+\alpha_2')}{z(z-\alpha_1)}, \tag{17}$$

where $\alpha_2'=e^{-(\frac{1}{2\tau_1}+j\omega_k)T_s}$. This model has the same poles than (3), but different numerator. To verify the validity of (17), the simulation performed to obtain the results shown in Fig. 2e was repeated using (17) instead of (3). The results of this simulation are shown in Fig. 2f. This figure shows that $\underline{e}^{\alpha\beta}(k)=0\ \ \forall k$, verifying the validity of (17). In order to evaluate the relative errors of each model, Fig. 3 shows outputs $\underline{i}^{\alpha\beta}_{Conv1}(kT_s)$ obtained through (2), (15), (3) and (17).

IV. Controller performance

In this section, the effect of using each model will be evaluated by implementing the current controller proposed in [1]. For simplicity, $T_d=T_s$ is considered, and the difference between using (2) or (15) to design the controller is evaluated. The transfer function of the controller proposed in [1] is:

$$R(z)=\frac{\underline{U}^{dq}_{\text{Conv,ref}}(z)}{\underline{I}^{dq}_{\text{Conv,err}}(z)}=\frac{\gamma}{K}\frac{z-\alpha_1}{z-1} \tag{18}$$

This article has been accepted for publication in a future issue of this journal, but has not been fully edited. Content may change prior to final publication. Citation information: DOI 10.1109/TPEL.2018.2841206, IEEE Transactions on Power Electronics

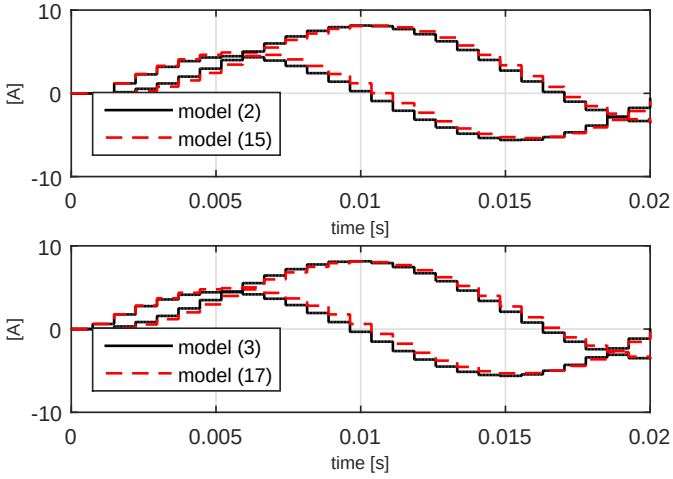

Fig. 3: Output $\underline{i}^{\alpha\beta}_{Conv1}(kT_s)$ for the different models.

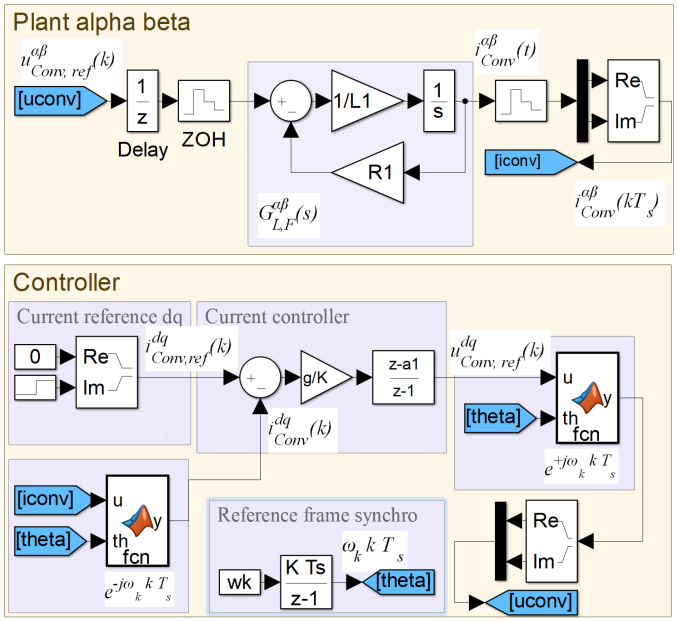

Fig. 4: Simulation block diagram.

where $\underline{I}^{dq}_{\text{Conv,err}}(z) = \underline{I}^{dq}_{\text{Conv,ref}}(z) - \underline{I}^{dq}_{\text{Conv}}(z)$, with $\underline{I}^{dq}_{\text{Conv,ref}}(z)$ the reference current, $0.25 \leq \gamma \leq 0.4$ a constant chosen by the designer, and $K = K_s$, with K_s defined in (2).

If the plant was actually modeled by (2), the closed loop system should show a perfect decoupling between axis d and q. In effect, considering (18) and (2), with $K = K_s$, results in the decoupled open loop transfer function [1]:

$$\underline{G}^{dq}_{\text{Open-Loop}}(z) = \frac{\gamma}{z(z-1)}. \tag{19}$$

However, simulation results show that the closed loop system is coupled. Figure 4 shows a simulation block diagram of the closed loop system. Figures 5a-b show current $\underline{i}^{dq}_{Conv} = i_d + ji_q$ (solid line) resulting from using this controller, with $\gamma = 0.35$ and $K = K_s$. In these simulations, the initial current reference is zero. At $t = 0.02$s a reactive current reference step $\underline{i}^{dq}_{Conv,ref} = 0 + j1$ is set (dashed line in Fig. 5a). As can be seen in Fig. 5a, this reference step in i_q results in a

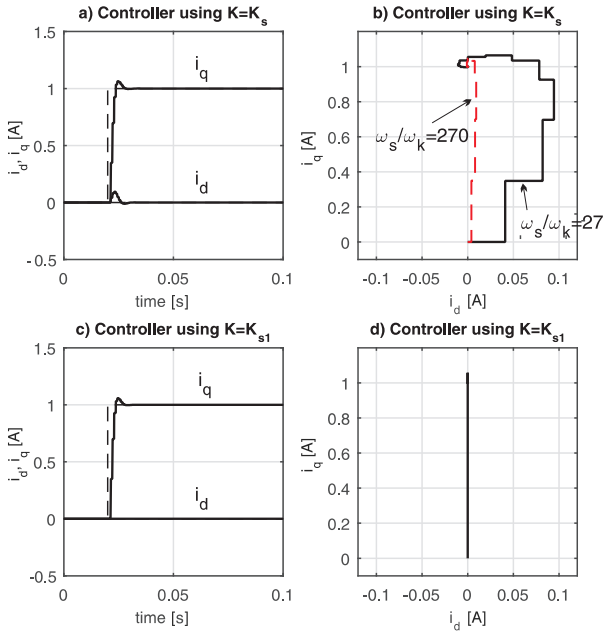

Fig. 5: Simulation result for $\gamma = 0.35$. a) Controller tuned with $K = K_s$, for K_s given in (2). b) Controller tuned with $K = K_{s1}$, for K_{s1} given in (15).

transient current in i_d, with a peak value of approximately 10% of the step value. This transient shows coupling between the axes, which is more noticeable in Fig. 5b (solid line). This coupling was previously identified in [1], and qualified as marginal. In [1] it is stated that the coupling is reduced by increasing the sampling frequency. This is verified in Fig. 5b (dashed line), where the simulation was performed with a sampling frequency ten times larger ($\omega_s/\omega_k = 270$). The coupling is the result of assuming that K_s in (2) is valid when designing the controller. To verify this assessment, Figs. 5c-d, show simulation results for the controller designed using $K = K_{s1}$, with K_{s1} defined in (15). Note that in both figures there is a perfect decoupling between axis d and q, which verifies the validity of model (15).

The system of Fig. 4 was implemented experimentally using a three-phase inverter with a 300V bus voltage. The parameters of the experiment were: $L_1 = 3.93mH$, $R_1 = 1.45\Omega$, $T_s = 100\mu$s and $\omega_s/\omega_k = 27$. Figure 6 shows the experimental results obtained when performing a step in current reference i_q from zero to 10A using the controller designed with $K = K_s$ and $K = K_{s1}$, both for $\gamma = 0.35$. The currents in the dq frame were captured from the internal registers of the digital signal processor used to implement the controller, while the abc currents were captured with an oscilloscope in high resolution mode. As can be seen, the experimental results match the simulation results of Fig. 5. Note that the coupling visible in Figs. 6d-e is within the steady state noise level.

V. Conclusions

This note identifies an improvement applicable for two discrete time models used in a recently published paper.

This article has been accepted for publication in a future issue of this journal, but has not been fully edited. Content may change prior to final publication. Citation information: DOI 10.1109/TPEL.2018.2841206, IEEE Transactions on Power Electronics

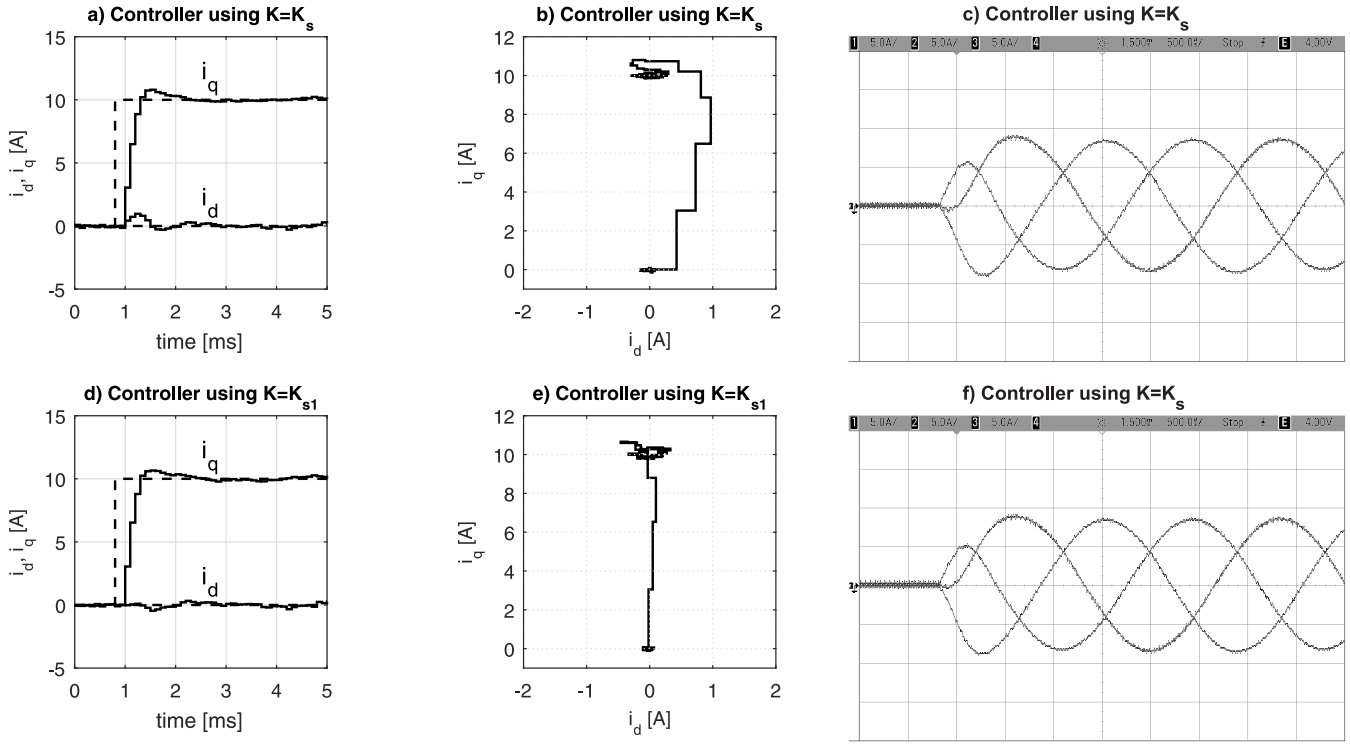

Fig. 6: Experimental results for $\gamma = 0.35$. a) Reference and measured currents in dq for $K = K_s$. b) i_d vs i_q for $K = K_s$. c) Phase currents for $K = K_s$ (5A/div, 500μs/div). d) Reference and measured currents in dq for $K = K_{s1}$. e) i_d vs i_q for $K = K_{s1}$. f) Phase currents for $K = K_{s1}$ (5A/div, 500μs/div).

The improved models are obtained following two alternative methods. The behavior of the resulting models was verified through simulations. The method used for the case where $T_d = T_s/2$, applies the discretization in the stationary $\alpha\beta$ frame, which makes the discretization process independent of the rotation speed of the rotating dq frame. The model in dq coordinates is then obtained simply by multiplying the constants of the $\alpha\beta$ model by proper rotation complex constants.

Additionally, it was verified that if the SRF-PI controller proposed in [1] is designed using the model proposed in that paper, the resulting closed loop controller has cross coupling in dq. On the other hand, it was shown that using the corrected model in the design yields a decoupled closed loop controller. These results were validated through both simulation and experimental results.

REFERENCES

[1] N. Hoffmann, F. W. Fuchs, M. P. Kazmierkowski, and D. Schröder, "Digital current control in a rotating reference frame - part I: System modeling and the discrete time-domain current controller with improved decoupling capabilities," *IEEE Transactions on Power Electronics*, vol. 31, no. 7, pp. 5290–5305, July 2016.

[2] J. Holtz, J. Quan, J. Pontt, J. Rodriguez, P. Newman, and H. Miranda, "Design of fast and robust current regulators for high-power drives based on complex state variables," *IEEE Transactions on Industry Applications*, vol. 40, no. 5, pp. 1388–1397, Sept 2004.

[3] C. L. Phillips and H. T. Nagle, *Digital Control System Analysis and Design (3rd Ed.)*. Upper Saddle River, NJ, USA: Prentice-Hall, Inc., 1995.

[4] F. Briz, M. W. Degner, and R. D. Lorenz, "Analysis and design of current regulators using complex vectors," *IEEE Transactions on Industry Applications*, vol. 36, no. 3, pp. 817–825, May 2000.

[5] H. Kim, M. W. Degner, J. M. Guerrero, F. Briz, and R. D. Lorenz, "Discrete-time current regulator design for ac machine drives," *IEEE Transactions on Industry Applications*, vol. 46, no. 4, pp. 1425–1435, July 2010.

[6] A. G. Yepes, A. Vidal, J. Malvar, O. López, and J. Doval-Gandoy, "Tuning method aimed at optimized settling time and overshoot for synchronous proportional-integral current control in electric machines," *IEEE Transactions on Power Electronics*, vol. 29, no. 6, pp. 3041–3054, June 2014.